Visuomotor integration is associated with zero time-lag synchronization among cortical areas

Pieter R. Roelfsema*†, Andreas K. Engel*, Peter König‡ & Wolf Singer*

* Max-Planck-Institute for Brain Research, Deutschordenstrasse 46, 60528 Frankfurt, Germany
† The Netherlands Ophthalmic Research Institute, and University of Amsterdam, Department of Medical Physics, P.O. Box 12141, 1100 AC Amsterdam, The Netherlands
‡ The Neurosciences Institute, 10640 John Jay Hopkins Drive, San Diego, California 92121, USA

INFORMATION processing in the cerebral cortex invariably involves the activation of millions of neurons that are widely distributed over its various areas. These distributed activity patterns need to be integrated into coherent representational states. A candidate mechanism for the integration and coordination of neuronal activity between different brain regions is synchronization on a fine temporal scale[1-3]. In the visual cortex, synchronization occurs selectively between the responses of neurons that represent related features[2-5] and that need to be integrated for the generation of coherent percepts; neurons in other areas of the cerebral cortex also synchronize their discharges[6-10]. However, little is known about the patterns and the behavioural correlates of synchrony among widely separated cortical regions. Here we report that synchronization occurs between areas of the visual and parietal cortex, and between areas of the parietal and motor cortex, in the awake cat. When cats responded to a sudden change of a visual pattern, neuronal activity in cortical areas exhibited synchrony without time lags; this synchrony was particularly strong between areas subserving related functions. During reward and inter-trial episodes, zero-time-lag synchrony was lost and replaced by interactions exhibiting large and unsystematic time lags.

The visual cortex is composed of a large number of areas[11,12], which contain neurons that are tuned to different visual features and that have different roles in the analysis of visual information[13]. Similar organizational principles hold for the parietal and the motor cortex, which also consist of numerous areas[11-16]. Any cerebral activity involves large numbers of areas, which must coordinate their activity. This coordination can be investigated by studying the correlations between field potentials, which reflect the average activity of large groups of neurons in the vicinity of a recording electrode[17]. The strength of coupling between transcortically recorded field potentials in different cortical areas changes dynamically during the performance of a behavioural task[10]. However, the spatial pattern of interactions between different areas and the time lags in these interactions have not yet been evaluated systematically.

Five cats were trained to press and release a lever with their forepaw in response to visual stimuli. At the onset of a behavioural trial, a grating was presented within a circular aperture. When the orientation of the grating changed, the cats had to respond by either pressing or releasing the lever, and were subsequently rewarded with food. When the cats performed this task reliably, transcortical electrodes were implanted under general anaesthesia. Coupling among transcortical field potentials that were recorded during the various episodes of the behavioural task was investigated using cross-correlation analysis.

Interactions between areas changed in a characteristic and highly reproducible manner during the course of the task. This is exemplified in Fig. 1 for the interaction between two areas of the parietal association cortex, area 7 and the lateral subdivision of area 5 (area 5l). During the entire task period, field potentials at the two recording sites were synchronized precisely, as indicated by a pronounced peak in the correlation function at zero time lag (Fig. 1a–c). The strength of this correlation varied between 24% and 33%, and was highest shortly after the cat pressed the response lever (Fig. 1b, e). The spacing of 46 ms between subsequent peaks of the correlation functions indicates that coupling was particularly strong for frequencies in the mid-beta frequency range (20–25 Hz), which dominate the power spectrum of the field potentials (Fig. 1f). During the reward period, large time lags of −7 to +50 ms occurred in the correlation function (Fig. 1d, e). This loss of zero-time-lag synchrony was associated with a strong increase of power in the alpha-band (7–13 Hz) (Fig. 1g).

A predominance of alpha-rhythms was a characteristic feature of the field potentials in all cats during the reward period (Fig. 2d). The amount of power in the alpha-band was on average more than fivefold greater during the reward period then when the animals paid attention to the visual stimuli ($P < 0.001$, U-test). Time lags in the correlation functions were compared between stimulus and reward periods for all area combinations exhibiting a robust interaction (Z-score > 6). On average, time lags in the interactions between areas were significantly smaller when the cats performed the task than during the reward period (Fig. 2d, $P < 0.00001$, U-test). When the cats were in the test box, but not involved in their task, low-frequency field-potential rhythms

TABLE 1 Strength of zero-time-lag synchronization between cortical areas

Areas	Correlation coefficient (%)	Range	N	Areas	Correlation coefficient (%)	Range	N
17c–7c	9 ± 4	4–14	4	5lc–4c	2 ± 3	0–5	2
17c–5lc	0		2	5lc–17i	0		2
17c–5mc	0		3	5lc–18i	4 ± 5	0–8	2
17c–4c	0		2	5lc–21i	4 ± 4	0–8	3
17c–17i	22 ± 7	12–28	4	5mc–4c	10 ± 1	9–11	2
17c–18i	12 ± 3	7–14	4	5mc–17i	0		3
17c–21i	8 ± 2	7–10	3	5mc–18i	0		3
7c–5lc	17 ± 10	10–24	2	5mc–21i	2 ± 3	0–6	4
7c–5mc	7 ± 2	6–9	3	4c–17i	0		2
7c–4c	0		2	4c–18i	0		2
7c–17i	6 ± 2	5–8	4	4c–21i	0		2
7c–18i	9 ± 5	5–15	4	17i–18i	20 ± 3	17–24	4
7c–21i	12 ± 2	9–14	3	17i–21i	21 ± 10	12–32	3
5lc–5mc	14 ± 6	9–21	3	18i–21i	15 ± 2	14–18	3

Correlation coefficients (±s.d.) are averaged across cats. Strenth of the zero-time-lag synchronization for the epochs when the cats waited for rotation of the grating. Abbreviations: i, areas ipsilateral to the forepaw used by the cats; c, areas contralateral to the forepaw used by the cats; N, number of cats.

FIG. 1 Changes in the interactions between cortical areas during task performance. a–d, Correlation functions between field potentials recorded in parietal area 7 and the lateral subdivision of area 5, averaged over trials. Black curves represent correlation functions that were computed for the following periods: a, when the cat waited for the appearance of the visual stimulus; b, an epoch shortly after the animal pressed the response lever; c, the phase in which the animal waited for the rotation of the stimulus; and d, the reward epoch. Curves on either side demarcate the 95% confidence interval of the correlation functions (±2 s.e.m.). Positive time lags in the correlograms indicate that activity in area 5l leads over activity in area 7. The ordinate shows correlation coefficients. e, Alterations in the average correlation function during the task. Abscissa, time relative to the behavioural event on which computational windows were aligned; ordinate, time lag of the correlation function. Computational windows were aligned on the onset of the visual stimulus in the first panel; on the pressing of the response key in the second panel; on the rotation of the grating in the third panel; and on the delivery of a food reward in the fourth panel. The computational windows corresponding to the correlation functions in (a–d) have been indicated below the respective panels. The colour scale indicates the Z-score of the correlation (value of the average correlation function normalized to the s.e.m.): red–yellow, positive correlations; green–blue, negative correlations. f, Power spectrum of the field potential recorded from area 7 (blue curve) and area 5l (red curve) in a 1-s window when the animal was pressing the response key. Lighter curves show the respective 95% confidence intervals. g, Power spectra at the two recording sites during the reward epoch (note the different scale on the ordinate). h, Location of the two recording sites in the left hemisphere. The location of the primary visual cortex (area 17) and the primary motor cortex (area 4) have been shaded.
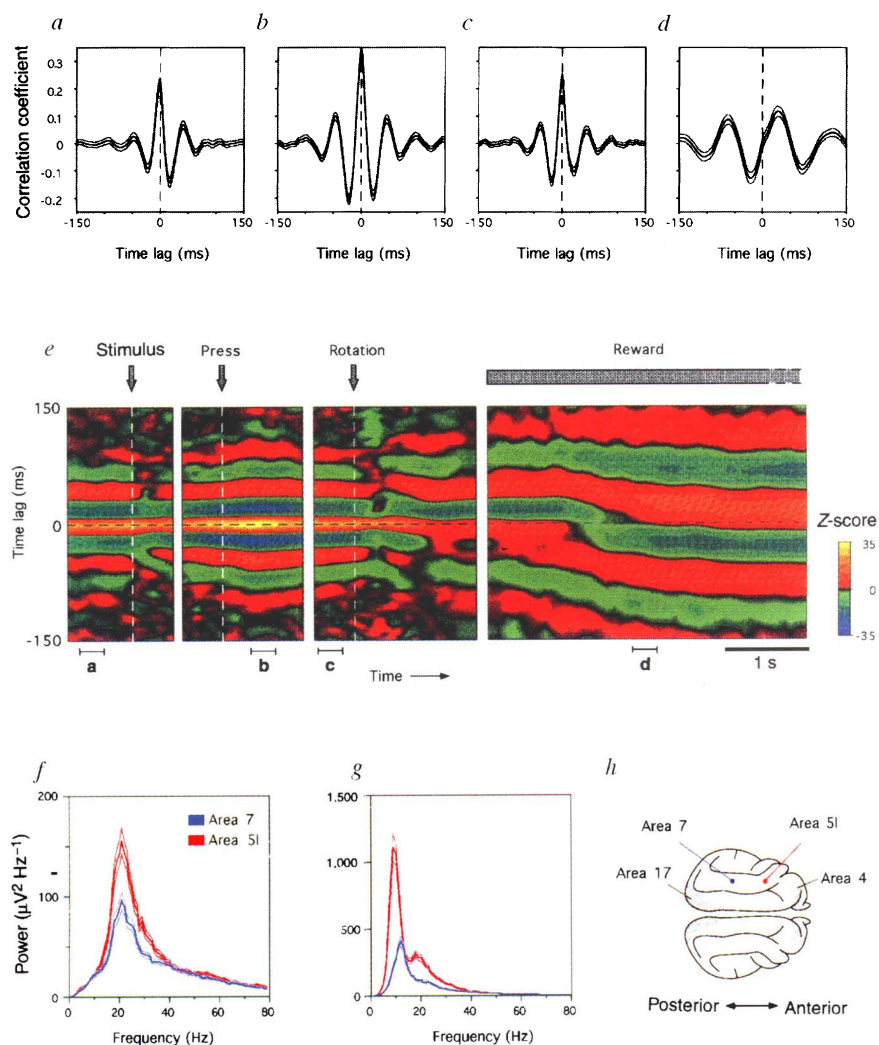
occurred spontaneously and were also associated with large time lags in the correlation functions. This indicates that synchrony among cortical areas is tighter when animals are engaged in a visuomotor task that requires attention and prompt reaction than when they are engaged in feeding or are at rest.

Correlations among field potentials recorded from areas of the visual, parietal and motor cortex when the cat was paying attention to the grating are shown in Fig. 2a. All significant interactions between areas consisted of synchrony with a time lag of approximately 0 ms (Fig. 2a, b, d). Significant synchronization occurred between area 17, the primary visual cortex, and area 7 of the parietal cortex. Area 7, in turn, exhibited significant synchronization with the lateral subdivision of area 5 and slightly weaker synchronization with the medial subdivision of area 5 of the parietal cortex. Conversely, area 4 of the motor cortex exhibited stronger synchronization with the medial than with the lateral subdivision of area 5. Thus synchronization did not occur between areas that are functionally remote (Fig. 2a). During the task period, the pattern of synchronization among visual areas was strongly dependent on the type of visual stimulation (Fig. 2b). When the visual stimulus was changed from a stationary to a moving grating, the strength of synchrony among visual areas increased by 23% on average. The interactions among areas of the parietal and motor cortex were not altered by this change of visual stimulus (Fig. 2b).

The average strength of zero-time-lag synchronization is listed for all combinations of investigated areas in Table 1 and shown schematically in Fig. 2c. This analysis shows that the strength of synchrony reflects the functional relations among cortical areas rather than their spatial vicinity, thus excluding current spread from remote sources as a cause for zero-time-lag synchrony. Synchronization between parietal area 7 and contralateral area 21, an area that occupies a relatively high position in the hierarchy of visual areas[11,12], was stronger than synchrony between area 7 and the ipsilateral primary visual cortex (area 17), despite the latter areas having a much smaller spatial separation (Table 1 and Fig. 2c).

In many cases, multi-unit activity (MUA), action potentials generated by local clusters of neurons, could be recorded through the transcortical electrodes. In these cases, coupling between MUA and field potentials was investigated by computing spike-triggered field-potential averages (STAs), which reveal the average field-potential fluctuation around the time that an action potential was recorded. The coupling between MUA recorded in parietal area 7 and field potentials that were recorded from the same electrode and from other electrodes in parietal area 5 and visual area 17 is shown in Fig. 3. During the trial, MUA in area 7 was synchronized to a sharp field-potential fluctuation at the same electrode with a time lag close to 0 ms (Fig. 3a, b). The STA during the reward period exhibited additional peaks with a spacing of ±100 ms, which indicates that the local cluster of neurons was entrained by the alpha-rhythm that occurred during feeding (Fig. 3c). The STAs for combinations of different areas did not reach statistical significance before the onset of the trial (Fig. 3a). Shortly after the cat pressed the response lever, however, the field potential in area 5 exhibited significant synchroni-

FIG. 2 Pattern of interactions among areas of the visual, parietal and motor cortex. *a*, Correlation functions among areas of the left hemisphere of one of the cats for the episode in which the animal was waiting for the rotation of the grating, averaged over trials. Positive time lags indicate lead of activity in the area shown on the left of the correlation functions over the area shown above the correlation functions. In all cats, recordings from somatosensory and motor areas were made in the hemisphere contralateral (c) to the paw that the animal used for pressing the lever; l, lateral; m, medial. *b*, Dependence of the correlation functions on the type of visual stimulation. Left, correlation functions obtained during visual stimulation with a stationary grating patch (18° of visual angle, 0.1 cycles deg^{-1}). Top row, correlation between field potentials in visual areas 18 and 21, ipsilateral (i) to the paw the cat used. Bottom row, correlations between field potentials in the lateral (5l) and medial (5m) subdivision of area 5 contralateral to the paw the cat used. Middle, correlation functions obtained during stimulation with a moving grating within a larger aperture (31° × 42°, 0.28 cycles deg^{-1}, 2.5 Hz). Synchronization between area 18 and area 21 was stronger during stimulation with the moving grating than during stimulation with the stationary grating ($P < 0.0001$, *U*-test). The strength of synchrony between the two subdivisions of area 5 was not affected by this change of the visual stimulus ($P > 0.5$). Right, location of all recording sites ipsilateral and contralateral to the paw the cats used. *c*, Synchronization strength among the areas from which recordings were obtained during the task period, averaged across cats. Lines between areas indicate the strength of synchrony. Thick lines indicate synchronization with a correlation coefficient exceeding 10%, thin lines interactions with a correlation coefficient between 5% and 10%, and broken lines interactions with a correlation coefficient smaller than 5%. Areas that are not connected did not exhibit significant synchronization in any of the cats (*Z*-score < 6). Areas in the hemisphere contralateral and ipsilateral to the paw the cats used are shown in the top and bottom row, respectively. Note that the interhemispheric asymmetry in the diagram reflects an asymmetry in electrode placement, not in the pattern of synchrony. *d*, Left, distribution of time lags in the correlation functions. Grey bars show time lags when the cats waited for the rotation of the grating, black bars show time lags during the reward epoch. Right, distribution of integrated power in the alpha frequency range (7–13 Hz) when the cats waited for rotation of the grating stimulus (grey bars) and in the reward epoch (black bars).
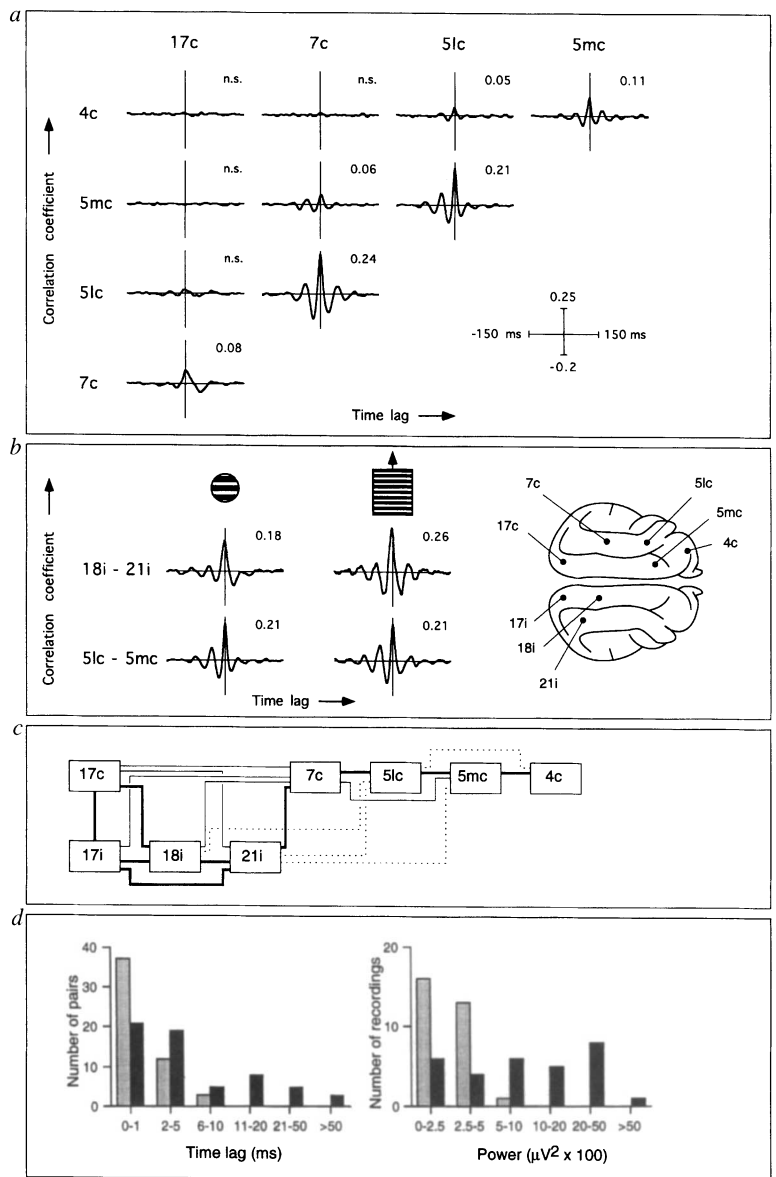
zation to the MUA in area 7 (Fig. 3*b*). During feeding, neurons in area 7 fired in synchrony with the alpha-rhythms occurring in area 17 and area 5, albeit at different phases (Fig. 3*c*). Neurons in area 7 did not exhibit large differences in firing rates between behavioural epochs (Fig. 3*d*). Nonetheless, the STAs revealed large changes between behavioural conditions in interactions both within (in accordance with ref. 9) and between areas. STAs could only be computed for electrode combinations for which MUA of sufficient quality was recorded. In these cases ($N = 39$), changes in the STAs closely resembled the changes in the correlations between field potentials, demonstrating that local clusters of neurons fired in synchrony with both the local and distant field-potential rhythms.

Synchronization among neuronal responses occurs within cortical regions as diverse as the visual[4,5], sensorimotor[6–8] and prefrontal cortex[9]. It has been shown that the strength of coupling between these widely spaced cortical areas changes dynamically during task performance[10]. Our results are in agreement with these findings, and demonstrate that, during attentive processing, interactions between areas are characterized by tight synchronization of activity with close to zero time lag. Moreover, in this behavioural state, zero-time-lag synchrony occurs not only among areas of the visual cortex[18–20], but also between areas of the visual and parietal cortex, and between areas of the parietal and motor

cortex. It has been suggested that zero-time-lag synchronization among the distributed responses of visual cortical neurons could serve their integration into coherent representational states[1–3]. If this is the case, the synchronization between neurons in parietal and motor cortical areas could, by analogy, serve to integrate distributed pre-movement activity into a coherent representation of a compound movement[21].

Synchrony between areas in different hemispheres has been shown to depend on the integrity of cortico-cortical connections[22,23], which suggests a minor contribution from subcortical projections. The scheme of coupling between areas suggested by our results is also in agreement with the pattern of cortico-cortical connections[11]. However, the dependence of the interactions among visual areas on the type of visual stimulation (Fig. 2*b*) demonstrates that the pattern of synchrony is not merely a reflection of the topology of connectivity between areas. This is in accordance with previous studies on the stimulus dependence of synchrony (reviewed in ref. 2). A similar conclusion follows from the drastic changes that occurred in the interactions during the course of a behavioural trial. Large time lags in the interactions between areas occurred only during the reward periods. The alpha-rhythms that characterize the cortical field potentials during feeding have been observed previously and were called 'post-reinforcement synchronization'[24], but phase relations

between field potentials in different areas during these rhythms had to our knowledge not been studied before.

The global changes in the pattern of interactions between areas may depend on the activity of modulatory projections that ascend from the brainstem, the basal forebrain and nonspecific thalamic nuclei. Activation of the mesencephalic reticular formation gives rise to behavioural arousal, increases the amount of power in the beta (15–30 Hz) and gamma (>30 Hz) frequency band of the EEG[25], and has been shown to enhance the occurrence of zero-time-lag synchronization of neuronal responses both within and across cortical areas[26,27]. Our results extend these findings by showing that such shifts in the pattern of interactions do not only occur during gross, long-term changes of vigilance, like the transition from sleeping to waking. Robust changes in interactions between areas also occur in relation to variations in the attentive state of awake animals during the repetitive alternation of reward episodes and episodes in which they have to be prepared to make a swift response to a visual stimulus. □

Methods

Behavioural task. The cats were kept unrestrained in a test box, the front of which consisted of a back-projection screen. Visual stimuli were generated with a d.c.-driven overhead projector and LCD display controlled by a personal computer. The cats were separated from the screen by a transparent response key. The cats were mildly food deprived (<10% weight loss) and trained to respond to a stationary, circular patch of grating (18° of visual angle, 0.1
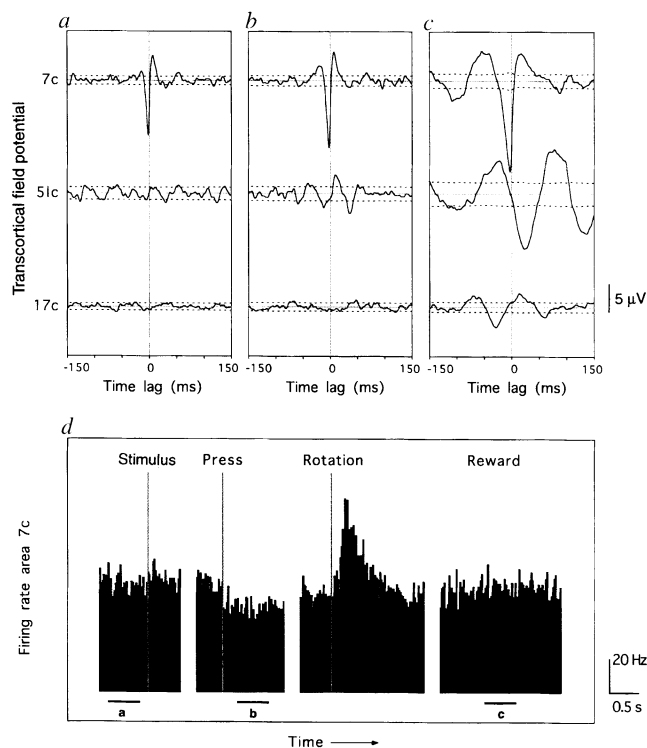

FIG. 3 Alterations in spike-triggered field-potential averages during the behaviour trial. *a–c*, Spike-triggered averages (STAs) obtained by correlating MUA in area 7 to the field potential at the same electrode (top trace), the field potential in area 5 (middle trace) and that in area 17 (bottom trace). STAs were computed: *a*, when the cat waited for the appearance of the visual stimulus; *b*, after the cat pressed the response lever; and *c*, in the reward epoch. Depth positivity (surface negativity) is plotted upwards. Stippled lines indicate the 95% confidence interval (±2 s.e.m.). *d*, Peri-stimulus time histogram of MUA in area 7. Spikes were aligned on the onset of the visual stimulus in the first panel, on the time that the response key was pressed in the second panel, on the rotation of the grating in the third panel, and on the delivery of the food reward in the fourth panel. Trigger spikes used for computation of the field-potential averages in (*a–c*) came from windows that are indicated below the respective panels.

cycles deg[−1]). Two cats responded to the grating stimulus by pressing the response lever, and holding the lever until the grating rotated by 90° or 180°, which occurred after 1–2.5 s. The rotation indicated that the key had to be released within 0.75 s. After correct performance the animals were rewarded with fluid cat food. For the other three cats the procedure was slightly modified to speed up learning: the onset of the grating stimulus indicated the start of a trial, but they only needed to respond to the rotation of the grating (after 2–4 s) by pressing the response key. All cats carefully attended the visual stimulus in the interval during which it was present.

Implantation of transcortical electrodes. Transcortical electrodes were implanted chronically under general anaesthesia, which was induced with ketamine and xylazine (10 and 2 mg per kg, intramuscular, respectively) and was maintained after intubation by ventilating the cat with a mixture of 70% N_2O and 30% O_2 supplemented with halothane (0.8–1.2%). Small trepanations were made and the dura was opened. Transcortical electrodes were composed of two teflon-coated platinum–iridium wires 120 μm in diameter. Insulation was removed over a distance of 80–120 μm, resulting in an impedance of 0.15–0.3 MΩ (at 100 Hz). The tip of the shorter wire was positioned in the superficial layers of the cortex, and the tip of the longer wire 1.8 mm deeper, in layer 6 or in the white matter. The electrode was glued to the pial surface with a small drop of tissue glue (cyanoacrylate), and the trepanation was closed with dental acrylic. Electrodes in area 4 were positioned in the representation of the contralateral forepaw[28], and electrodes in visual cortical areas according to retinotopic maps. Electrode positioning in areas 7 and 5 was guided by cytoarchitectonic maps. Electrodes were positioned at the same stereotactic coordinates in all cats. The cats were allowed to recover for at least 14 days before data collection. After completion of the recording sessions, the cats were killed with an overdose of pentobarbital and perfused transcardially. The positions of the recording sites were confirmed in Nissl-stained sections.

Correlation analysis. Cats completed on average 78 successful trials per day, and recording sessions were continued until data from at least 600 trials were obtained. Transcortical potentials were amplified differentially and filtered between 5 and 100 Hz. For computation of the correlation functions, data segments of different trials were first aligned on the events that occurred during the course of a trial (onset and rotation of the grating, time of key-press and onset of the reward epoch). Correlation functions were calculated for each trial in successive computational windows of 300 ms duration that overlapped each other by 200 ms. Subsequently, these correlation functions were averaged over trials and the variance was computed at each point of the correlation functions. Z-scores were obtained by dividing the average correlation functions by the s.e.m. Correlation functions with $Z > 6$ were considered to be significant (two-sided *t*-test, $P < 0.0005$ after correction for multiple comparisons (301 points per correlation function times 80 correlation functions) by the Bonferroni method). To estimate the volume of cortex that contributed to the signals recorded by a transcortical electrode, cats were anaesthetized with a mixture of 70% N_2O and 30% O_2 supplemented with halothane (0.4%), and paralysed with pancuronium bromide (0.15 mg per kg body weight per hour). Evoked potentials to a patch of square-wave grating (spatial frequency, 0.59 cycles deg[−1]; size, 1.7° × 1.7°) that reversed phase at 10 Hz were recorded from the transcortical electrodes in area 17. At a receptive field eccentricity of 3° the amplitude of the evoked potential was reduced to less than 50% when the grating patch was shifted by 1.7°. Taking the cortical magnification factor at this eccentricity into account[29], this shift corresponds to a cortical distance of less than 1.5 mm. Because the minimal distance between transcortical electrodes was 5 mm, a contribution of current spread (volume conduction) to the correlation functions can be excluded. The same conclusion follows from the fact that correlation functions exhibited small time lags and asymmetrical satellite peaks during the task period and larger time lags during the reward period, even for the electrode combinations with the smallest separation. In Fig. 2*b*, for example, the field potential in area 18 exhibited a small (2 ms) time lead over that in area 21, and asymmetrical satellite peaks occurred in the correlation function between the lateral and medial subdivision of area 5. Because volume-conducted sources would have contributed without time lag to both recording sites that were subjected to correlation analysis, the observed time lags and asymmetrical satellite peaks exclude a volume-conducted contribution to the correlation functions.

Spike-triggered field-potential averages (STAs). Although electrodes remained *in situ* for more than 6 months, stable MUA recordings with a signal-to-noise ratio larger than 3 were obtained from some of the wires. STAs were computed for the spikes in windows of 500 ms duration in successive trials from a single recording day. On average, correlations among field potentials were more pronounced than those revealed by STAs in inter-areal combinations. Several factors probably contribute to this difference. First, changes in the trigger levels for spike detection and small drifts in the position of the wires precluded pooling of STAs over days, whereas correlations between field potentials were highly reproducible and could be pooled. Second, MUA reflects only suprathreshold activity of cells near the electrode tip, whereas field potentials result from the average sub- and supra-threshold responses of neurons within a cortical volume with radius over several hundred micrometres (ref. 17). Third, field potentials are biased towards representing activity that is locally synchronous[1], whereas MUA recordings are unbiased in this respect. It

seems likely that these sampling differences account for the observed difference in the strength of correlations revealed by the two measures.

1. Abeles, M. *Corticonics* (Cambridge Univ. Press, 1991).
2. Singer, W. & Gray, C. M. *Annu. Rev. Neurosci.* **18**, 555–586 (1995).
3. Engel, A. K., König, P., Kreiter, A. K., Schillen, T. B. & Singer, W. *Trends Neurosci.* **15**, 218–226 (1992).
4. Gray, C. M., König, P., Engel, A. K. & Singer, W. *Nature* **338**, 334–337 (1989).
5. Eckhorn, R. *et al. Biol. Cybern.* **60**, 121–130 (1988).
6. Bouyer, J. J., Montaron, M. F. & Rougeul, A. *Electroencephalogr. Clin. Neurophysiol.* **51**, 244–252 (1981).
7. Murthy, V. N. & Fetz, E. E. *Proc. Natl Acad. Sci. USA* **89**, 5670–5674 (1992).
8. Sanes, J. N. & Donoghue, J. P. *Proc. Natl Acad. Sci. USA* **90**, 4470–4474 (1993).
9. Vaadia, E. *et al. Nature* **373**, 515–518 (1995).
10. Bressler, S. L., Coppola, R. & Nakamura, R. *Nature* **366**, 153–156 (1993).
11. Scannell, J. W., Blakemore, C. & Young, M. P. *J. Neurosci.* **15**, 1463–1483 (1993).
12. Felleman, D. J. & Van Essen, D. C. *Cereb. Cortex* **1**, 1–47 (1991).
13. Maunsell, J. H. R. & Newsome, W. T. *Annu. Rev. Neurosci.* **10**, 363–401 (1987).
14. Goodale, M. A. & Milner, A. D. *Trends Neurosci.* **15**, 20–25 (1992).
15. Kalaska, J. F. & Crammond, D. J. *Science* **255**, 1517–1523 (1992).
16. Jeannerod, M., Arbib, M. A., Rizzolatti, G. & Sakata, H. *Trends Neurosci.* **18**, 314–320 (1995).
17. Mitzdorf, U. *Physiol. Rev.* **65**, 37–100 (1985).
18. Engel, A. K., Kreiter, A. K., König, P. & Singer, W. *Proc. Natl Acad. Sci. USA* **88**, 6048–6052 (1991).
19. Frien, A., Eckhorn, R., Bauer, R., Woelbern, T. & Kehr, H. *Neuroreport* **5**, 2273–2277 (1994).
20. Nelson, J. I., Salin, P. A., Munk, M. H. J., Arzi, M. & Bullier, J. *Vis. Neurosci.* **9**, 21–37 (1992).
21. Roelfsema, P. R., Engel, A. K., König, P. & Singer, W. *J. Cogn. Neurosci.* **8**, 603–625 (1996).
22. Engel, A. K., König, P., Kreiter, A. K. & Singer, W. *Science* **252**, 1177–1179 (1991).
23. Munk, M. H. J., Nowak, L. G., Nelson, J. I. & Bullier, J. *J. Neurophysiol.* **74**, 2401–2414 (1995).
24. Buchwald, N. A., Horvath, F. E., Wyers, E. J. & Wakefield, C. *Nature* **201**, 830–831 (1964).
25. Steriade, M., McCormick, D. A. & Sejnowski, T. J. *Science* **262**, 679–685 (1993).
26. Munk, M. H. J., Roelfsema, P. R., König, P., Engel, A. K. & Singer, W. *Science* **272**, 271–274 (1996).
27. Steriade, M., Amzica, F. & Contreras, D. *J. Neurosci.* **16**, 392–417 (1996).
28. Nieoullon, A. & Rispal-Padel, L. *Brain Res.* **105**, 405–422 (1976).
29. Tusa, R. J., Palmer, L. A. & Rosenquist, A. C. *J. Comp. Neurol.* **177**, 213–236 (1978).

In vivo dendritic calcium dynamics in neocortical pyramidal neurons

Karel Svoboda, Winfried Denk, David Kleinfeld*
& David W. Tank

Biological Computation Research Department, Bell Laboratories, Lucent Technologies, Murray Hill, New Jersey 07974, USA

THE dendrites of mammalian pyramidal neurons contain a rich collection of active conductances that can support Na$^+$ and Ca^{2+} action potentials (for a review see ref. 1). The presence, site of initiation, and direction of propagation of Na$^+$ and Ca^{2+} action potentials are, however, controversial[2], and seem to be sensitive to resting membrane potential, ionic composition, and degree of channel inactivation, and depend on the intensity and pattern of synaptic stimulation. This makes it difficult to extrapolate from *in vitro* experiments to the situation in the intact brain. Here we show that two-photon excitation laser scanning microscopy[3] can penetrate the highly scattering tissue of the intact brain. We used this property to measure sensory stimulus-induced dendritic [Ca^{2+}] dynamics of layer 2/3 pyramidal neurons of the rat primary vibrissa (Sm1) cortex *in vivo*. Simultaneous recordings of intracellular voltage and dendritic [Ca^{2+}] dynamics during whisker stimulation or current injection showed increases in [Ca^{2+}] only in coincidence with Na$^+$ action potentials. The amplitude of these [Ca^{2+}] transients at a given location was approximately proportional to the number of Na$^+$ action potentials in a short burst. The amplitude for a given number of action potentials was greatest in the proximal apical dendrite and declined steeply with increasing distance from the soma, with little Ca^{2+} accumulation in the most distal branches, in layer 1.

* Present address: Department of Physics 0319, University of California, La Jolla, California 92093, USA.

This suggests that widespread Ca^{2+} action potentials were not generated, and any significant [Ca^{2+}] increase depends on somatically triggered Na$^+$ action potentials.

Although *in vivo* experiments provided some of the first evidence for active currents in dendrites[1], most of our understanding of the presence and role of these dendritic currents comes from *in vitro* brain-slice experiments using electrophysiological recording and optical imaging of [Ca^{2+}]. Such experiments have provided increasing evidence that Na$^+$ action potentials can, under appropriate conditions, propagate centrifugally into the dendritic tree of cortical pyramidal neurons[4]. Because these action potentials open voltage-dependent Ca^{2+} channels[5–8] and modulate voltage-dependent synaptic currents[9], they could be important in the control of long-term synaptic plasticity. Brain-slice experiments have also demonstrated Ca^{2+} action potentials in pyramidal cell dendrites[10,11] associated with very large dendritic Ca^{2+} accumulations[6,12]. However, dendritic excitability is strongly affected by a variety of biophysical parameters, such as ionic composition[13]. Furthermore, the site of dendritic action-potential initiation depends on the strength of synaptic excitation[8,14], and the activation of voltage-dependent conductances can be modulated by inhibitory synaptic inputs[15–17]. This implies that it is difficult to extrapolate from *in vitro* experiments to the intact nervous system. Thus understanding the presence and biological function of active dendritic currents requires measurements of membrane voltages[18] and dendritic ion dynamics in the intact nervous system in response to behaviourally relevant stimuli.

We measured [Ca^{2+}] dynamics in neocortical neurons of anaesthetized rats by using a two-photon laser scanning microscope (TPLSM)[3] that allows imaging while the membrane potential is recorded using a microelectrode (Fig. 1a). In our TPLSM, two infrared photons produced by a mode-locked pulsed laser are simultaneously absorbed to excite fluorophores that normally absorb at visible wavelengths, with an absorption rate proportional to the square of the incident light intensity. Two-photon excitation was important for this experiment for several reasons[19]. First, infrared excitation provides greater depth penetration into the cortex than does visible light. Second, excitation is localized to the focal region (excitation volume $\sim 1\,\mu m^3$), providing three-dimensional optical sectioning and resolution equivalent to that of a confocal microscope without any loss of fluorescence light due to a detector pinhole, resulting in much reduced phototoxicity and photobleaching. Regular spiking[20] pyramidal cells in layer 2/3 of the primary vibrissa cortex (Sm1) were penetrated with sharp microelectrodes, and were iontophoretically filled with calcium green-1 (Fig. 1b). Dendrites were clearly resolved down to 500 μm below the pial surface, and three-dimensional cell morphology and location of electrode penetration could be reconstructed from stacks of images acquired at different depths (Fig. 1c). For [Ca^{2+}] measurements at selected locations with high temporal resolution, line-scan mode was used[9].

Trains of whisker deflections (5 Hz, 2 s) produced a sequence of electrical events consisting of slow depolarizations, during which one, two or no Na$^+$ action potentials occurred (Fig. 1d–f). All slow depolarizations with Na$^+$ action potentials were quite large with low amplitude variability (Fig. 1e, f), whereas most that did not contain Na$^+$ action potentials were smaller and more variable in amplitude. The largest slow depolarizations ranged from 10 mV when recorded in the soma, to 40 mV when recorded in dendrites. Although they resembled large excitatory postsynaptic potentials[21], the uniformity of slow depolarizations associated with Na$^+$ action potentials also suggests that regenerative voltage-dependent conductances are involved. Simultaneous microelectrode measurements of membrane potential and fluorescence measurements of calcium indicator-filled dendrites ($n = 49$) revealed [Ca^{2+}] transients that occurred in one-to-one correspondence with Na$^+$ action-potential bursts, with more action potentials leading to larger [Ca^{2+}] transients (Fig. 1d–f, arrows). The transients had fast rise times (~ 2 ms) and short decay-time constants (< 100 ms).